A *Ka*-Band GaN-on-Si MMIC Analog Vectorial Modulator and Its Broadband Calibration Procedure

G. Collodi, *Member, IEEE*, M. Passafiume, *Member, IEEE*, T. Bilotta, and A. Cidronali, *Senior Member, IEEE*

***Abstract*— This letter introduces for the first time a fully integrated analog vectorial modulator (VM) in gallium nitride on silicon (GaN-on-Si) monolithic microwave-integrated circuit (MMIC) technology, operating in *Ka*-band, and an analytical calibration technique suitable for VM. An extensive characterization of the prototype, with both static and dynamic modulating signals, validates both the design and the calibration technique. The VM is capable to produce corrected constellations with accuracy of 0.06 dB and 0.28° root mean square, respectively, for amplitude and phase, across the 35–40 GHz bandwidth. Furthermore, it is capable to generate single-side modulated signal with undesired sideband suppression in excess of 47 dBc.**

***Index Terms*— Front-end, gallium nitride on silicon (GaN-on-Si), millimeter-wave (mm-w), multifunction monolithic microwave-integrated circuit (MMIC), vectorial modulator (VM).**

I. Introduction

THE increasing interest on multifunctions systems in gallium nitride (GaN) technology at millimeter-wave (mm-w) [1], drives the developments of mm-w front-end key functions in this semiconductor technology. Among the several building blocks that compose a front end, the vectorial modulator (VM) assumes particular relevance for both communications transceivers [2], and radar front end [3].

In this context, the letter novelty is twofold. The authors introduce the first GaN on silicon (GaN-on-Si) high electron mobility transistor (HEMT) technology implementation of the VM architecture discussed in [4], for *Ka*-band applications. More relevantly, the authors derive a calibration procedure allowing the VM to produce an almost perfect signal modulation, when driven by a corrected set of control signals.

II. MMIC GaN-on-Si Vector Modulator

The VM is implemented by a pair of biphase balanced modulators driven in quadrature by a Lange coupler and combined in phase by a Wilkinson combiner. Within the balanced modulator, the two reflection-type modulators are driven with complimentary signal $(\overline{Vi}; Vi)$ and $(\overline{Vq}; Vq)$.

Manuscript received December 31, 2020; accepted January 18, 2021. Date of publication February 8, 2021; date of current version April 8, 2021. This work was supported by the National Italian Research Project, under Grant PRIN-2015 no. 2015CPC2MA. *(Corresponding author: A. Cidronali.)*

The authors are with the Department of Information Engineering, University of Florence, 50139 Florence, Italy (e-mail: alessandro.cidronali@unifi.it).

Color versions of one or more figures in this letter are available at https://doi.org/10.1109/LMWC.2021.3054463.

Digital Object Identifier 10.1109/LMWC.2021.3054463

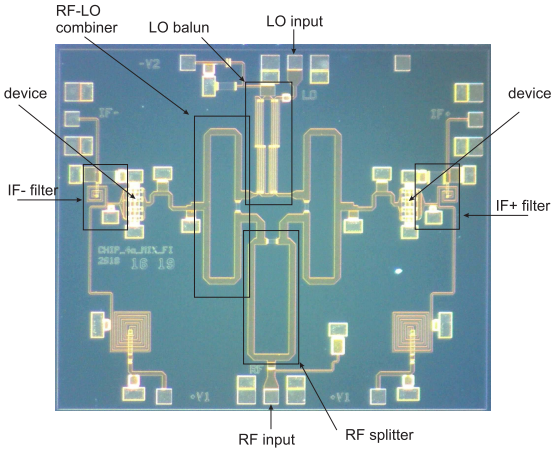

Fig. 1. Vector modulator prototype chip photograph.

This specific topology permits to remove the residual imperfection of the tuning loads, and overall possible differences between active devices due to spread of their pinchoff voltage. The VM prototype was developed by the OMMIC foundry process GaN-on-Si HEMT 100-nm process (D01GH). The main function of the active device consists of the drain–source impedance variation in cold-FET configuration. The use of GaN-on-Si HEMTs biased at zero drain–source voltage (cold-FET), as variable loads, exploits their inherent higher linearity of dc-I–V characteristic in linear region, when compared with GaAs HEMT devices [5]. The tradeoff, within the design frequency range 35–40 GHz, between device output conductance and parasitic capacitance led to the selection of the device geometry, that is 2 fingers 25 μm wide. The photography of the monolithic microwave-integrated circuit (MMIC) prototype is shown in Fig. 1. It is a 2.5 mm $\times$ 2 mm die with ground-signal-ground (GSG) probe contacts and pads for the signal controls. The latter are not shunted by capacitors and thus are available to control the VM dynamically; in addition, they include a resistor pad that provides a divide-by-two factor to the applied external voltage. The Lange coupler and the Wilkinson combiner were extensively optimized by electromagnetic simulators, using the process simulation data provided by the foundry.

III. Calibration of the Vector Modulator

Although the VM topology provides some robustness with respect to the several impairments that might be related to the tuning loads, it is affected by higher order nonidealities.

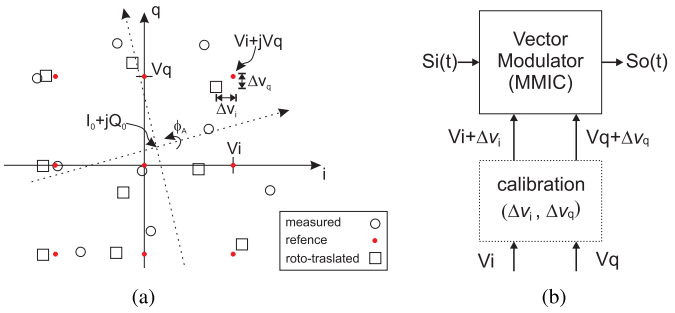

Fig. 2. Vector modulator calibration conceptualization: definition of correction parameters Δv_I and Δv_Q. (a) Roto-translation of measured symbols. (b) Calibrated VM diagram.

For these reasons, the VM could exhibit a not symmetrical constellation, cfr. Fig. 2(a), when driven by a symmetric set of control in-phase and quadrature (IQ) signals; thus it is important to introduce a VM calibration procedure.

According to Fig. 2(b), the calibration enables the control of the VM with a proper pair of corrected IQ signals (i.e., $V_I + \Delta v_I, V_Q + \Delta v_Q$), which slightly differ from the set of nominal signals and permits to correct the distorted modulation. In the previous literature [6], this procedure was defined by an extensive optimization procedure, while in this letter we introduce an analytical procedure based on the measured set of symbols, which provides the theoretically exact calibration of the VM. The calibration procedure considers only the characterization of the S21 parameter across the control voltages and frequency domains. It assumes the measured S21 differentiable within the entire set of control voltage domain, and it is developed as it follows. Let's define the VM input signal $s_I(t) = S \cdot e^{j2\pi f_{\mathrm{RF}} t + \phi_0}$ where f_{RF} is the carrier frequency, ϕ_0 the reference phase of the input signal, and S the constant amplitude of the carrier. The ideal operation of the VM consists in impressing on to the carrier a complex ideal envelope $e_I(t) = V_I(t) + jV_Q(t)$ in fact, due to the impairments, the actual measured envelope results

$$e_A(t) = g(V_I(t), \quad V_Q(t))e^{j\phi_A} + (I_0 + jV_0) \tag{1}$$

where $g(i, q)$ is a nonlinear function with respect to (V_I, V_Q), $e^{j\phi_A}$ is a rotation term, and $(I_0 + jV_0)$ a shift on the complex envelope domain $(V_I + jV_Q)$ space; the two latter mentioned parameters are functions of the carrier frequency, f_{RF}. The VM calibration process starts from the compensation of both the rotation and the shift terms; this can be effectively actuated by the following two steps. Once the constellation on the phase plane of e_A is characterized, its reference $(I_0 + jV_0)$ can be estimated as its mean value, while the actual rotation ϕ_A, can be found by differentiating e_A in the phase plane. This procedure leads to the estimation of a new version of the envelope $\hat{e_A}(i, q)$, which is centered and aligned on the Cartesian (i, q) plane. The next step of the calibration procedure sets the following identity:

$$\hat{e_A}\big(V_I + \Delta v_I, V_Q + \Delta v_Q\big) = k \cdot \big(V_I + jV_Q\big) \tag{2}$$

with $\Delta v_I, \Delta v_Q$ real values to be identified. In (2), the right-hand side (r.h.s.) represents the ideal constellation in the codomain of the VM operation, which is expected to be proportional to the VM input modulating signal domain. The proportionality constant, k, is to be adjusted according to the magnitude of the S21 parameter. Under the basic assumption that $\hat{e_A}(i, q)$ is first-order differentiable about (V_I, V_Q), we can derive

$$\hat{e_A}\big(V_I + \Delta v_I, V_Q + \Delta v_Q\big) = \hat{e_A}\big(V_I, \ V_Q\big) + \nabla \hat{e_A}(i, \ q)\big|_{V_I, \ V_Q} \cdot \begin{pmatrix} \Delta v_I \\ \Delta v_Q \end{pmatrix} \tag{3}$$

where

$$\nabla \hat{e_A}(i, q) = \left(\frac{\partial \hat{e_A}}{\partial i}, \frac{\partial \hat{e_A}}{\partial q} \right) \tag{4}$$

developing further (2)

$$\begin{aligned} \Re\big\{\hat{e_A}\big(V_I + \Delta v_I, V_Q + \Delta v_Q\big)\big\} &= kV_I \\ \Im\big\{\hat{e_A}\big(V_I + \Delta v_I, V_Q + \Delta v_Q\big)\big\} &= kV_Q \end{aligned} \tag{5}$$

and rewriting (5) by using (3), in matrix notation

$$\begin{bmatrix} \Re\left\{ \dfrac{\partial \hat{e_A}}{\partial i}\big|_{V_I, V_Q} \right\} & \Re\left\{ \dfrac{\partial \hat{e_A}}{\partial q}\big|_{V_I, V_Q} \right\} \\ \Im\left\{ \dfrac{\partial \hat{e_A}}{\partial i}\big|_{V_I, V_Q} \right\} & \Im\left\{ \dfrac{\partial \hat{e_A}}{\partial q}\big|_{V_I, V_Q} \right\} \end{bmatrix} \cdot \begin{bmatrix} \Delta v_I \\ \Delta v_Q \end{bmatrix} = \begin{bmatrix} kV_I - \Re\big\{\hat{e_A}\big(V_I, V_Q\big)\big\} \\ kV_Q - \Im\big\{\hat{e_A}\big(V_I, V_Q\big)\big\} \end{bmatrix}. \tag{6}$$

In (6), the r.h.s. is totally determined by the real and imaginary parts of the complex envelope and by the coordinate of each constellation point, that is (kV_I, kV_Q). As well as, the 2×2 matrix in the left-hand side (l.h.s.) of (6) is calculated by the partial derivatives of $\hat{e_A}(i, q)$. The characterization of these terms through the entire domain of (V_I, V_Q), and within the design frequency band, permits the calculation of the correction terms $\Delta V_I(V_I, V_Q, \omega)$ and $\Delta V_Q(V_I, V_Q, \omega)$.

IV. Experimental Validation

A. Static VM Prototype Characterization

The prototype S-parameters were characterized in the 35–40-GHz frequency band with control voltage spanning from 0 to −3.4 V step 0.2 V, which reflects to an actual HEMT gate control from 0 to −1.7 V step 0.1 V due to the internal 1:2 resistor divider. The S21 parameter is reported in the linear polar plots of Fig. 3, respectively, at the frequencies of 35 and 40 GHz, where the data are compared with the respective simulated ones; the minimum insertion loss is of 13.7 dB. The plots exhibit a constellation of symbols, which is a common representation of the VM performance. The constellations appear distorted at the border and not uniformly distributed in the phase. The accuracy of the simulations in terms of mean square error (MSE) is 6.6E−5 across the design bandwidth. Fig. 4 reports the comparison of simulated and measured data for four symbols at the corner of the constellation in the design frequency range. In this case the accuracy, reported in term of normalized MSE as the symbols have the same nominal magnitude, results 5.1E−3.

B. Validation of the VM Calibration

The calibration technique discussed in Section III was applied to the measured data set of Fig. 3. The resulting calibrated data shown the almost ideal constellation reported in Fig. 5, which exhibits a slight reduction of the maximum amplitude at the higher frequency; the accuracy of the calibrated constellation, calculated with respect an ideal grid of symbols, is respectively, for amplitude and phase 0.06 dB

TABLE I

PERFORMANCE SUMMARY OF REPORTED VM, IMPLEMENTED IN III–V COMPOUND SEMICONDUCTOR HEMT

Ref.	[4]	[7]	[8]	[9]	[this work]
Technology	$0.25\mu m$ GaAs	50 nm GaAs	$0.15\mu m$ GaAs	$0.15\mu m$ GaAs	$0.1\mu m$ GaN-on-Si
Frequency (GHz)	30-40 and 55-65	235 and 270	45-75	40	35-40
architecture	quad.-balanced	quad. var. gain$^{(3)}$	quad.-balanced	quad.-balanced	quad.-balanced
Phase error (deg)	± 2	$< 12.5^{(1)}$	$< 0.6^{(1)}$	± 1.5	$6.38^{(1)}, 0.28^{(2)}$
Magnitude error	$\pm 0.3dB$	$< 1.8dB^{(1)}$	$< 3^{(1)}$	$\pm 0.3dB$	$2.80dB^{(1)}, 0.06dB^{(2)}$
Modulation	256-QAM 1Mbps	QAM	QPSK	QAM	256-QAM
Calibration	n.a.	n.a.	voltage converter incl.	n.a.	yes
Side-band suppr.	n.a.	n.a.	n.a.	n.a.	$> 34dBc^{(4)}, > 47dBc^{(5)}$ at 3 MHz

(1) raw, and (2) after calibration, RMS error data; (3) active structure, (4) before and (5) after calibration.

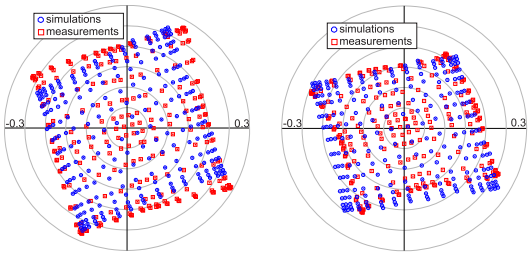

Fig. 3. Comparison between measured and simulated S21 symbols for the entire span of control: $Vi = [-3.4{:}0.2{:}0.0]$; $Vq = [-3.4{:}0.2{:}0.0]$. (a) 35 GHz. (b) 40 GHz.

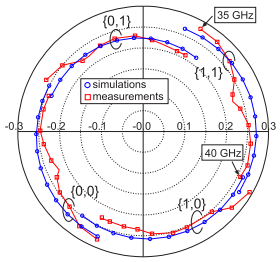

Fig. 4. Comparison between measured and simulated S21 symbols $\{1,1\} = [-3.4,-3.4]V$, $\{1,0\} = [-3.4,0]V$, $\{0,1\} = [0,-3.4]V$, $\{0,0\} = [0,0]V$ versus frequency range 35–40 GHz.

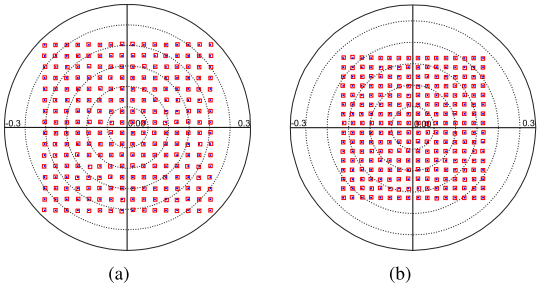

Fig. 5. Measured 256-QAM constellation after calibration; measured S21 data (square), symbols reference grid (dots). (a) 35 GHz. (b) 40 GHz.

and 0.28° root mean square (rms). The independent validation of the calibration technique considers the dynamic case of a modulating signal pair, $V_I(t)$ and $V_Q(t)$, capable to complex modulate the carrier by the signal $\exp(j2\pi f_1 t)+\exp(j2\pi f_2 t)$. In this experiment, we considered a signal source at 37.5 GHz and the two-tone modulating signals at $f_1 = 3.25$ MHz and $f_2 = 3.75$ MHz. The experiment assumes that the VM operates in quasi-static regime. The expected modulated signal spectrum consists of the single-sideband, while the measured

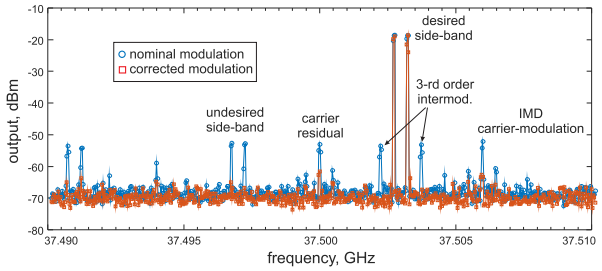

Fig. 6. Modulated two-tone single-side spectrum, $f_1 = 3.25$ MHz and $f_2 = 3.75$ MHz, with and without calibration. Input power of 0 dBm at carrier.

spectra with and without the correction are shown in Fig. 6. The resulting spectrum without correction, contains the undesired sideband due to the imperfect constellation along with a significant third-order intermodulation. When the calibration is inserted the spectrum contains only the right-sideband and a residual carrier, while both the side bands and the third-order intermodulation are below the noise. The intermodulation distortion (IMD) was evaluated for a number of ten samples belonging to the same wafer, and across the frequency range; it was verified an average IMD of -44.2 dB with a variance of 4.7 dB. With respect to temperature variation, by experimental tests and simulations analysis at 37.5 GHz on a typical sample, we observed a 256-quadratic-amplitude modulation (QAM) constellation variation within -34 dB across the temperature range -20 °C to $+80$ °C.

V. CONCLUSION

The letter has introduced a comprehensive, theoretically exact, calibration technique for the correction of the circuit impairments affecting the modulated signals. The letter also has introduced an analog vector modulator operating in *Ka*-band developed in GaN-on-Si MMIC technology. The VM prototype was extensively characterized and, when corrected by the calibration terms, it provides a static constellation amplitude and phase accuracy, respectively, of 0.06 dB and 0.28° rms, across 35–40 GHz. As independent validation of the calibration technique and the capability of the VM prototype a two-tone signal was adopted as modulating signal, the resulting modulated signal exhibited an undesired left-sideband rejection in excess of 47 dBc.

The comparison with state-of-the-art VM is provided in Table I, where VM sharing comparing architectures are considered. The proposed work exhibits the better in its class amplitude and phase accuracy when calibrated with the proposed method.

REFERENCES

[1] R. Rieger, A. Klaassen, P. Schuh, and M. Oppermann, "GaN based wideband T/R module for multi-function applications," in *Proc. Eur. Microw. Conf. (EuMC)*, Sep. 2015, pp. 514–517.

[2] S. Maddio, A. Cidronali, and G. Manes, "Real-time adaptive transmitter leakage cancelling in 5.8-GHz full-duplex transceivers," *IEEE Trans. Microw. Theory Techn.*, vol. 63, no. 2, pp. 509–519, Feb. 2015.

[3] K. Lin, Y. E. Wang, C.-K. Pao, and Y.-C. Shih, "A *K*a-band FMCW radar front-end with adaptive leakage cancellation," *IEEE Trans. Microw. Theory Techn.*, vol. 54, no. 12, pp. 4041–4048, Dec. 2006.

[4] A. E. Ashtiani, S.-I. Nam, A. d'Espona, S. Lucyszyn, and I. D. Robertson, "Direct multilevel carrier modulation using millimeter-wave balanced vector modulators," *IEEE Trans. Microw. Theory Techn.*, vol. 46, no. 12, pp. 2611–2619, Dec. 1998.

[5] M. S. Clements, A.-V. Pham, J. S. Sacks, B. C. Henderson, and S. E. Avery, "Comparison of highly linear resistive mixers in depletion and enhancement mode GaAs and GaN pHEMTs at *Ka* band," in *IEEE MTT-S Int. Microw. Symp. Dig.*, Jun. 2018, pp. 435–438.

[6] D. S. McPherson and S. Lucyszyn, "Vector modulator for *W*-band software radar techniques," *IEEE Trans. Microw. Theory Techn.*, vol. 49, no. 8, pp. 1451–1461, Aug. 2001.

[7] D. Muller, A. Tessmann, A. Leuther, T. Zwick, and I. Kallfass, "A *H*-band vector modulator MMIC for phase-shifting applications," in *IEEE MTT-S Int. Microw. Symp. Dig.*, May 2015, pp. 1–4.

[8] D. Zhang *et al.*, "A 45–75 GHz vector modulator MMIC with built-in voltage converter," *IEEE Microw. Wireless Compon. Lett.*, vol. 27, no. 5, pp. 515–517, May 2017.

[9] Y. Hou, L. Li, R. Qian, and X. Sun, "An efficient technique for designing high-performance millimeter-wave vector modulators with low temperature drift," *IEEE Trans. Microw. Theory Techn.*, vol. 56, no. 12, pp. 3100–3107, Dec. 2008.